Sinkholes in Wink, Texas, Observed by Satellite Radar Imagery

Jin Woo Kim and Zhong Lu
Roy M. Huffington Department of Earth Sciences,
Southern Methodist University, Dallas, Texas

ABSTRACT.—Two sinkholes in Wink, Texas (Wink Sinks #1, #2), collapsed in 1980 and 2002, respectively. The area where the sinkholes are located in Winkler County, west Texas, is underlain by thick salt beds at depth of about ~400 m. Anthropogenic activities related to oil and water production have been considered as a primary cause of the sinkhole development and creation. Previous studies have suggested that poor wellbore management, which failed to prevent the intrusion of freshwater and/or unsaturated saltwater into soluble rocks, resulted in the cavity formation, roof failure, and successive upward cavity migration. Interferometric synthetic aperture radar (InSAR) measurements using Advanced Land Observation Satellite Phased Array type L-band Synthetic Aperture Radar and TerraSAR-X images during 2007–2011 and 2015–2016 revealed fine spatial details about the progression of the existing sinkholes and neighboring regions. The immediate vicinities of both existing sinkholes are still subsiding, albeit at a decreasing rate, from ~18 cm/yr in 2011 to about ~8 cm/yr in 2016, possibly because of the gradual deposit of the debris from overlying rock formation into the cavity. However, an alarming rate of subsidence can be found ~1 km east of Wink Sink #2. The peak subsidence rate of this area ranged from ~40 cm/yr during 2007–2011 to more than 60 cm/yr during 2015–2016. Although the initial trigger of the subsidence feature over the area 1 km east of Wink #2 might be similar to that of Wink Sinks #1 and #2 (i.e., poor borehole management, water-flooding operations in a karst environment), the recent expansion and accelerated subsidence may be attributed to the severe drought in 2011. Continuous monitoring of the subsidence in the broader vicinity of the Wink sinkholes is needed for preventing future catastrophic outcomes of long-term developing geohazards to the area's oil production facilities, infrastructure, and human safety.

INTRODUCTION

Sinkholes, depressions or holes caused by collapse of land surface, are a major geohazard in karst environments worldwide (Beck and Pearson, 1995; Johnson and Neal, 2003; Gutiérrez and others, 2014). Sinkholes are generally formed when evaporite, carbonate, or gypsum rocks in karst terrains dissolve because of chemical or other processes that result in the development of underground cavities, failures of overlying sediments/rocks, upward cavity migration, and surface depression and collapses.

Well-known sinkholes in the world can be found over the coasts of the Dead Sea, northeastern Spain, the Netherlands, and North America (e.g., Baer and others, 2002; Galve and others, 2009; Chang and Hanssen, 2014; Paine and others, 2012; Jones and Blom, 2014; Kim and others, 2016; Kim and Lu, 2018). In the United States, 48 out of 50 states have karst terrains with most of the damaging sinkholes located along the Gulf Coast states including Texas, Louisiana, and Florida, among others (Kuniansky and others, 2016).

Sinkholes can be induced by both natural processes and anthropogenic activities. Recent studies provided evidence that the vast majority of newly formed sinkholes are of anthropogenic origins, including aquifer exploitation and mining dewatering resulting in water level decline, water impoundment and injection, and vegetation removal among others (Waltham and others, 2005; Kim and others, 2019). Impacts caused by sinkhole activities include economic losses and damage to infrastructure (Kuniansky and others, 2016). Because of the increasing demand for water and energy resources,

Kim, Jin Woo; and Lu, Zhong, 2021, Sinkholes in Wink, Texas, Observed by Satellite Radar Imagery, *in* Johnson, K. S.; Land, Lewis; and Decker, D. D. (eds.), Evaporite Karst in the Greater Permian Evaporite Basin (GPEB) of Texas, New Mexico, Oklahoma, Kansas, and Colorado: Oklahoma Geological Survey, Circular 113, p. 105–110.

it is anticipated that negative effects of sinkhole hazards will grow in the future.

Two cover-collapse sinkholes, namely Wink Sinks #1 and #2, in west Texas, collapsed in 1980 and 2002, respectively (Figure 1). These two sinkholes are located in a region underlain by the Salado Formation on the eastern edge of the Delaware Basin. Wink Sink #1 was created on 3 June 1980 and enveloped an abandoned plugged oil well that produced oil from 1928 to 1951 and became inactive after 1964. Wink Sink #2, formed on 21 May 2002, centered on a water-supply well. Past investigations suggest these two sinkhole collapses were associated with intense hydrocarbon drilling and production activities in the Hendrick oilfield that caused the salt dissolution, cavity formation, roof failure, upward cavity migration, and surface collapse (Johnson and others, 2003; Johnson, 2005; Kim and others, 2019).

Here we report on the evolution of the ground surface deformation over the area including and surrounding both Wink sinkholes using radar remote sensing images acquired by satellites during 2007 to 2011 and 2015 to 2016. Our goal is to assess the state of the ground surface subsidence over this sinkhole-prone area using high-spatial-resolution satellite observations, which provides a scientific basis for the need to mitigate potential sinkhole hazards.

DATA AND ANALYSIS

SAR and InSAR data

Interferometric synthetic aperture radar (InSAR) combines two or more synthetic aperture radar (SAR) images of the same imaging geometry from the same area to produce an interferogram (a.k.a. InSAR image) (e.g., Massonnet and others, 1993; Zebker and others, 1994; Rosen and others, 2000; Hanssen, 2001; Lu and Dzurisin, 2014). The interferometric phase, after the correction of topographic effect with the aid of a digital

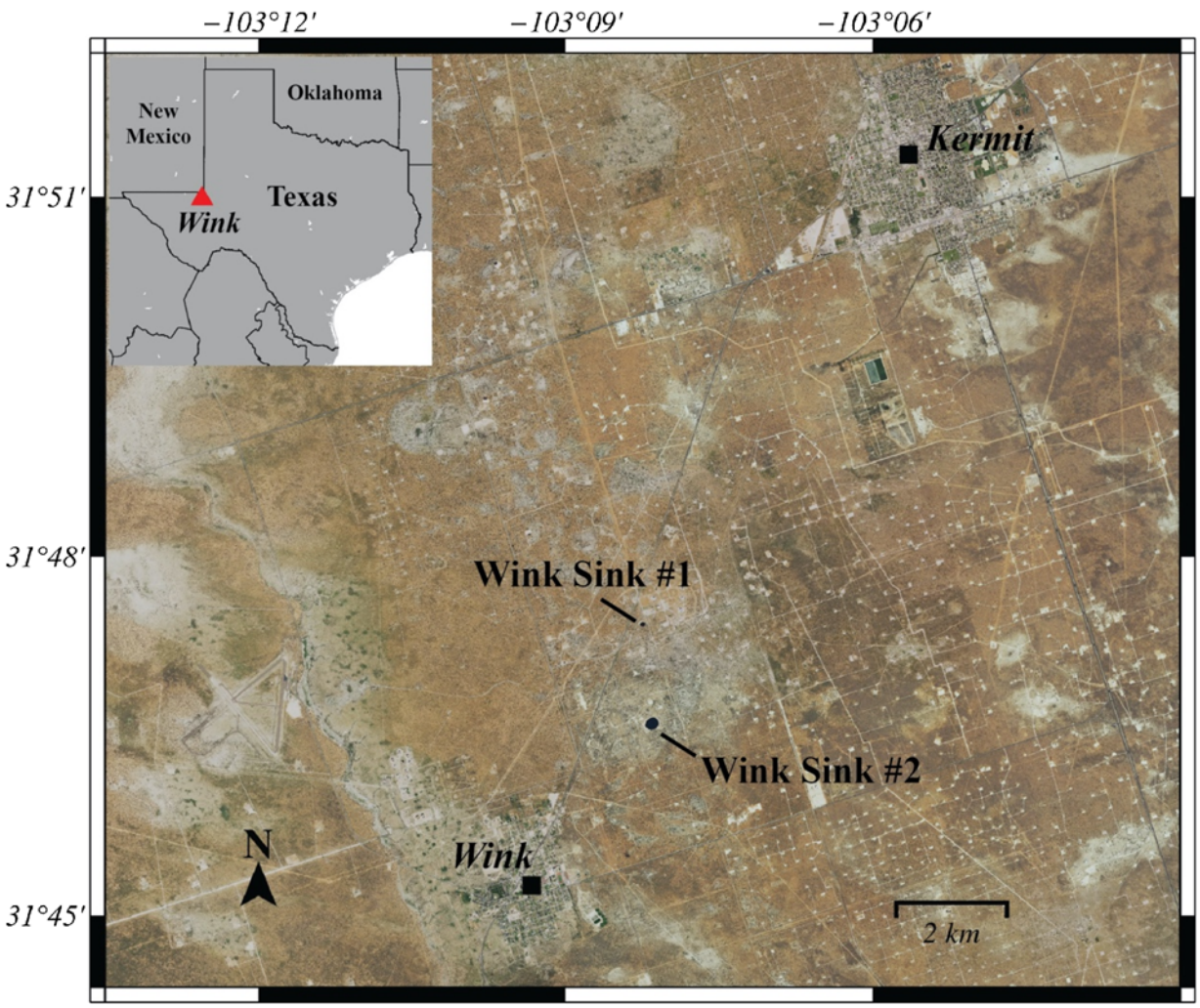

Figure 1. Location of Wink sinkholes near Wink in west Texas. Wink Sink #1, created in 1980, is located ~1.5 km north of Wink Sink #2, which formed in 2002. Wink Sinks #1 and #2 have a dimension of 80 m × 110 m and 200 m ×250 m, respectively.

elevation model, presents the range (the distance from the satellite to ground) change that includes subtle ground deformation and atmosphere artifacts and other noise. InSAR data, combined with geophysical modeling, have been used to characterize geohazards associated with volcanoes, landslides, earthquakes, and land subsidence among others (Lu and others, 2010). To improve the precision of InSAR measurements, multitemporal InSAR images are needed to obtain high temporal coherence and reduce atmospheric artifacts through time-series InSAR processing (e.g., Ferretti and others, 2001; 2011; Hooper and others, 2004; Lu and Zhang, 2014; Qu and others, 2015).

Two data sets are used in this report: L-band (wavelength of ~24 cm) Advanced Land Observation Satellite (ALOS) Phased Array type L-band Synthetic Aperture Radar images acquired from January 2007 to January 2011 by the Japan Aerospace Exploration Agency(JAXA) and X-band (wavelength 3.1 cm) high-resolution TerraSAR-X images acquired from October 2015 to March 2016 by the German Aerospace Center (DLR). The detailed characteristics of these SAR images can be found in Lu and Zhang (2014). The ALOS stripmap-mode SAR images have spatial resolutions of 10 to 20 m, whereas the TerraSAR-X spotlight-mode images used in this study have a spatial resolution of ~25 cm. The mean deformation rate from each satellite data set is obtained by stacking multiple coherent interferograms (Kwoun and others, 2006). As the observed ground deformation associated with sinkhole development is dominated by the vertical displacement (Kim and Lu, 2018), we convert the line-of-sight deformation into the vertical displacement to facilitate the evaluation of the evolution of the observed deformation.

Observed deformation

Based on the average subsidence rate map from ALOS data during 2007 to 2011, we can identify several subsidence cones (Figure 2). The first feature is the subsidence radiating about 600-m outward from Wink Sink #1. The subsidence peaks at a rate of ~12 cm/yr, located about ~100 m to the west of Wink Sink #1 (Figure 2). The second subsidence feature of an ellipsoid shape (500 m × 400 m in dimension) can be identified about ~500 m to the north of Wink Sink #2, with a peak subsidence of ~18 cm/yr (Figure 2). The third and the most prominent subsidence feature is located about 1 km east of Wink Sink #2. It resembles a tooth rotated sideway: the subsidence at the south peak, about 200 m northwest of the intersection of county roads 201 and

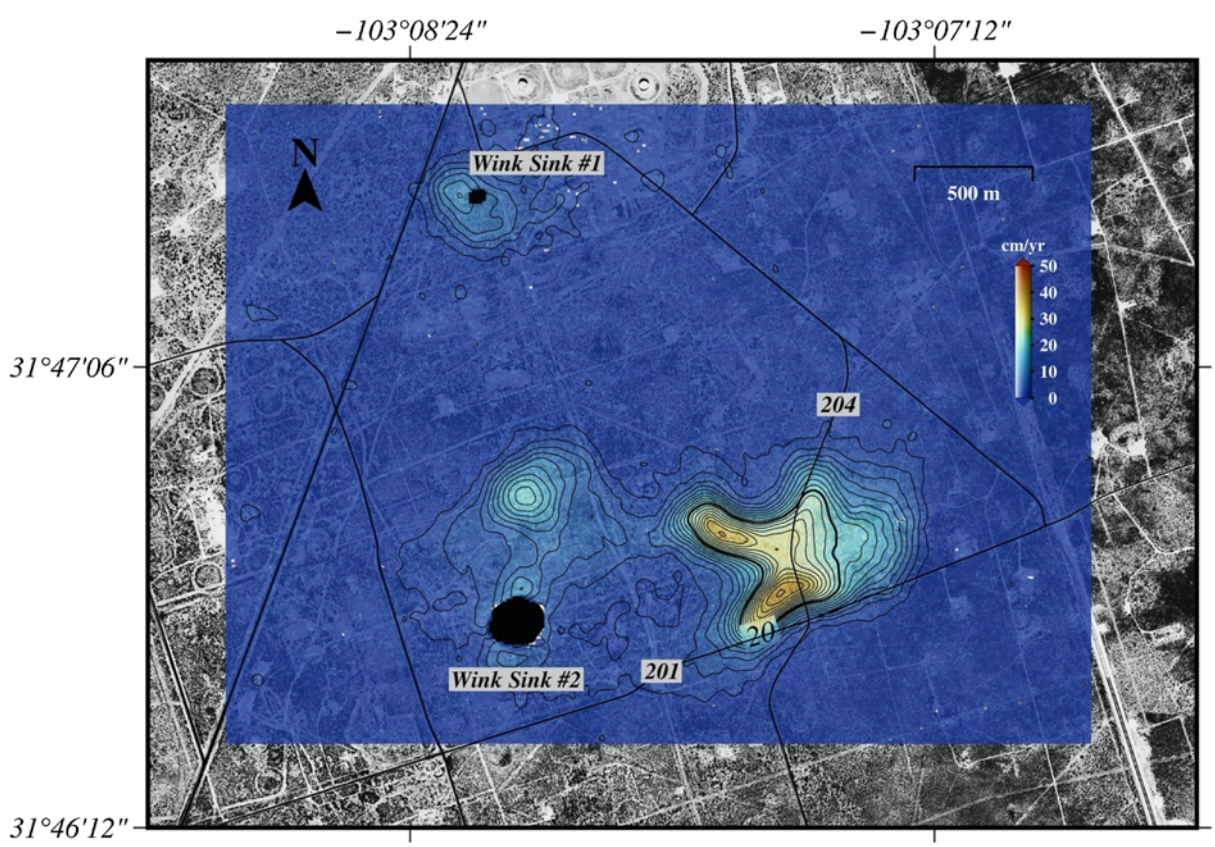

Figure 2. Average subsidence rate map from ALOS PALSAR images from January 2007 to January 2011. Contour lines are drawn at intervals of 2 cm/yr.

204, was about 40 cm/yr, whereas it was 35 cm/yr at the north peak (Figure 2).

The subsidence rate map for 2015 to 2016 from TerrraSAR-X images shows that the three subsidence features as seen during 2007 to 2011 changed over time to some degree (Figure 3). The subsidence rates at the first feature (i.e., near Wink Sink #1) and the second feature (north of Wink Sink #2) reduced to 4 and 4–8 cm/yr, respectively (Figure 3), and the extents of subsidence also shrank. However, the third and most prominent feature about 1 km east of Wink Sink #2 changed significantly. There were two distinct subsidence troughs in 2015 to 2016. The subsidence rate over the north peak reduced to about 26 cm/yr, whereas it increased to more than 60 cm/yr over the south peak located on county road 201, about 100 m west of the intersection of the county roads 201 and 204 (Figure 3). It is obvious the peak subsidence increased in magnitude from 2011 to 2015–2016 and that the location of the peak subsidence migrated southward.

DISCUSSION AND CONCLUSION

The subsidence observed near the existing Wink Sinks #1 and #2 suggests the underground cavity around each was continuously filled with debris from upper formations. This void filling process, called a suffusion, produced continuous surface subsidence over the newly formed sinkholes in the early stage of each sinkhole's collapse (Waltham and others, 2005; Kim and others, 2019). The subsidence rates and dimensions surrounding Wink Sinks #1 and #2 reduced over time, suggesting the two existing sinkholes stabilized as a consequence of nearly fully filled cavities (Waltham and others, 2005; Kim and others, 2019).

The double-peak subsidence feature about 1 km east of Wink Sink #2 manifests as alarming sinkholes under development, with the peak subsidence reaching more than 60 cm/yr during 2015 to 2016 near the intersection of county roads 201 and 204. The triggering mechanism for the observed subsidence has also been attributed to dissolution of the Salado Formation around ~400 m deep, similar to the cause of collapses at Wink Sinks #1 and #2 (Paine and others, 2012; Kim and others, 2016, 2019). There were numerous water wells and hydrocarbon-production wells, most of which have been inactive and abandoned. Inappropriate borehole management, as judged by current more stringent standards, could initiate the freshwater contact of the Salado layer through unplugged boreholes, corroded pipes, or leaked casing and other engineering issues (Paine and

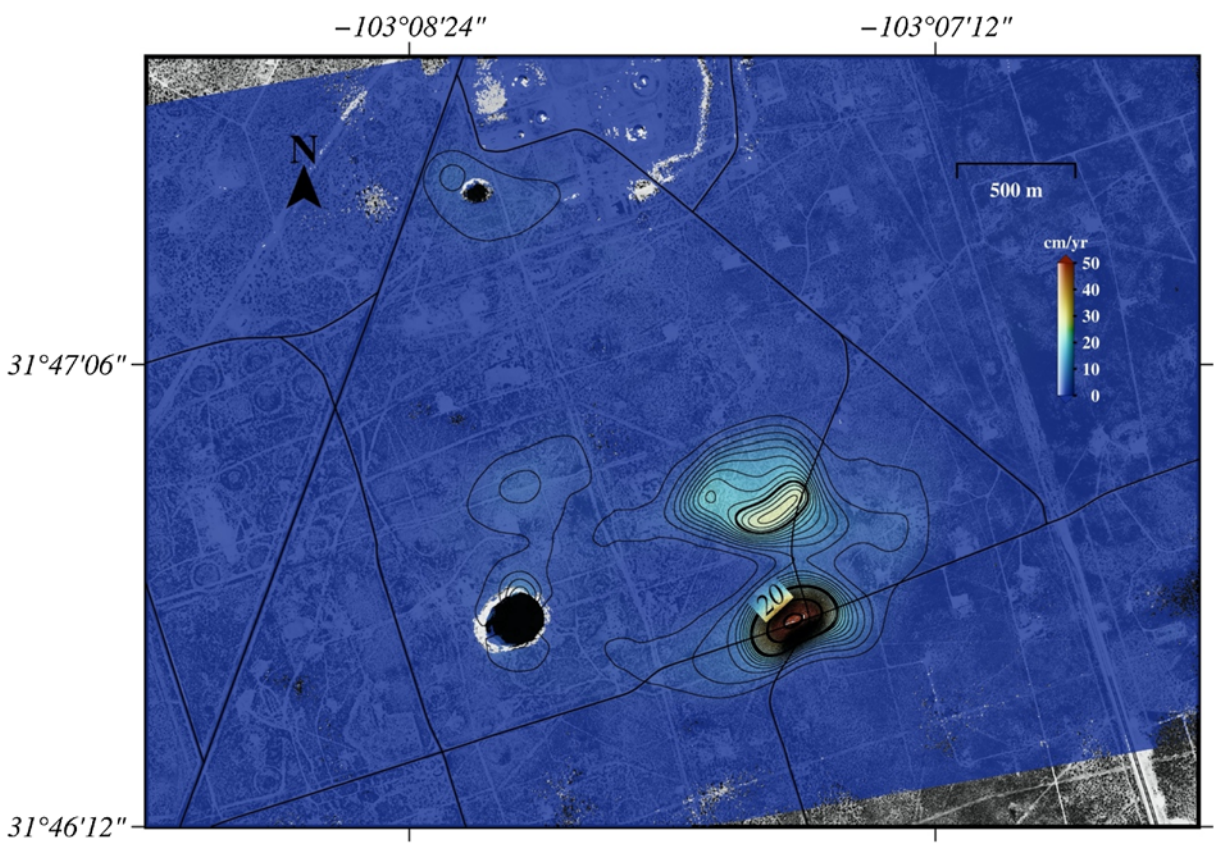

Figure 3. Average subsidence rate map from TerraSAR-X images from October 2015 to March 2016. Contour lines are drawn at intervals of 2 cm/yr.

others, 2012; Kim and others, 2016, 2019). In addition, intensive water-flooding operations were used in this area for several decades from the 1970s to the 2000s (Kim and others, 2019), which could act as an important contributor to the rapid subsidence. Fractures in the aquifer and formations surrounding the salt layer created by pressurized fluid injection and long-term hydrocarbon production could have allowed freshwater to intrude into the Salado Formation, initiating the dissolution process (Kim and others, 2019). The accelerated salt dissolution could cause cavity formation, upward migration, and the ground surface subsidence. Therefore, we believe the combined effects of improper borehole management and massive water production were responsible for the development of the subsidence feature east of Wink Sink #2.

Inspecting the deformation over the double-peak subsidence feature east of Wink Sink #2 suggests that not only did the rate of peak subsidence increase, but that the extent of the subsidence also expanded from 2007–2011 to 2015–2016 (Figures 2 and 3). For example, the peak subsiding area was contained to the north of county road 201 in 2007–2011, but expanded further south of county road 201 in 2015 to 2016. Kim and others (2019) attributed the accelerated subsidence at the developing sinkholes to a combination of human-induced (hydrocarbon and water flooding, etc.) and natural perturbations (droughts) in the subsurface surrounding the Salado layer. In fact, a severe drought hit the area in 2011, which was the worst in the past 30 yr in Texas (Kim and others, 2019). Because of decadal water-flooding operations that caused fractures in the formations surrounding the Salado Formation along with those formed during borehole drilling and realignment (Heithecker, 1932; Adams, 1944; Baumgardner and others, 1982; Johnson, 1989; Kim and others, 2019), the area already possessed a well-developed fracture system. The 2011 drought lowered groundwater levels, which in turn added overburden stress, and further compounded sinkhole development vulnerability. The increased effective stress and internal erosion in the overlying layers can result in more rapid downward percolation of freshwater in aquifer systems into the underlying salt beds, causing the acceleration of the salt dissolution and surface/subsurface subsidence (Linares and others, 2017; Kim and others, 2019). Although the double-peak subsidence feature has not yet resulted in a collapse as witnessed at Wink Sinks #1 and #2, the accelerated subsidence represents a significant potential geohazard in the area. Hence, continuous monitoring of the subsidence in the vicinity of the Wink sinkholes using satellite InSAR or other ground-based instruments is urgently needed to prevent future catastrophic outcomes that will endanger the area's oil production facilities, critical infrastructure, and human safety.

ACKNOWLEDGEMENTS

This work was supported in part by the NASA Earth Surface and Interior Program under Grants 80NSSC19K1491 and NNX16AL10G and in part by the Shuler-Foscue Endowment at Southern Methodist University.

REFERENCES CITED

Adams, J.E., 1944, Upper Permian Ochoan Series of Delaware Basin, west Texas and southeastern New Mexico: American Association of Petroleum Geologists, Bulletin, v. 28, p. 1596-1625.

Baer, G., Schattner, U., Wachs, D., Sandwell, D., Wdowinski, S., and Frydman, S., 2002, The lowest place on Earth is subsiding – an InSAR (interferometric synthetic aperture radar) perspective: Geological Society of America, Bulletin, v. 114, no. 1, p. 12-23.

Baumgardner, R.W., Hoadley, A.D., and Goldstein, A.G., 1982, The Wink Sinks; a case history of evaporite dissolution and catastrophic subsidence: Formation of the Wink Sink, a salt dissolution and collapse feature, Winkler County, Texas: Bureau of Economic Geology, The University of Texas at Austin, Report of Investigations No. 114, 38 p.

Beck, B.F., and Pearson, F.M., 1995, Karst Geohazards: Engineering and environmental problems in karst terrane, *in* Proceedings of the Fifth Multidisciplinary Conference on Sinkholes and the Engineering and Environmental Impact of Karst, Gatlinburg, Tennessee, 2–5 April 1995: Balkema, Rotterdam, 582 p.

Chang, L., and Hanssen, R.F., 2014, Detection of cavity migration and sinkhole risk using radar interferometric time series: Remote Sensing of Environment, v. 147, p. 56-64.

Ferretti, A., Prati, C., and Rocca, F., 2001, Permanent scatterers in SAR interferometry: IEEE Transactions on Geoscience and Remote Sensing, v. 39, p. 8-20.

Ferretti, A., Fumagalli, A., Novali, F., Prati, C., Rocca, F., and Rucci, A., 2011, A new algorithm for processing interferometric data-stacks: SqueeSAR: IEEE Transactions on Geoscience and Remote Sensing, v. 49, no. 9, p. 3460-3470.

Galve, J. P., Gutiérrez, F., Remondo, J., Bonachea, J., Lucha, P., and Cendrero, A., 2009, Evaluating and comparing methods of sinkhole susceptibility mapping in the Ebro Valley evaporite karst (NE Spain): Geomorphology, v. 111, no. 3/4, p. 160-172.

Gutiérrez, F., Parise, M., De Waele, J., and Jourde, H., 2014, A review on natural and human-induced geohazards and impacts in karst: Earth-Science Reviews, v. 138, p. 61-88.

Hanssen, R.F., 2001, Radar interferometry: data interpretation and error analysis: New York, Boston,

Dordrecht, London, Moscow, Kluwer Academic Publisher, 308 p.

Heithecker, R.E., 1932, Some methods of separating oil and water in west Texas fields, and the disposal of oil-field brines in the Hendrick Oil Field, Texas: US Bureau of Mines, Report of Investigations 3173, 16 p.

Hooper, A., Zebker, H., Segall, B., and Kampes, B., 2004, A new method for measuring deformation on volcanoes and other natural terrains using InSAR persistent scatterers: Geophysical Research Letters, v. 31, L23611, 5 p.

Johnson, K.S., 1989, Development of the Wink Sink in west Texas, U.S.A., due to salt dissolution and collapse: Environmental Geology and Water Sciences, v. 14, no. 2, p. 81-92.

Johnson, K.S., and Neal, J. T., 2003, Evaporite karst and engineering/environmental problems in the United States: Oklahoma Geological Survey, Circular 109, 353 p., ISSN 0078-4397.

Johnson, K.S., Collins, W.W., and Seni, S. J., 2003, Sinkholes and land subsidence due to salt dissolution near Wink, West Texas, and other sites in western Texas and New Mexico: Oklahoma Geological Survey, Circular 109, p.183–195.

Johnson, K.S., 2005, Subsidence hazards due to evaporite dissolution in the United States: Environmental Geology, v. 48, p. 395-409.

Jones, C.E., and Blom, R.G., 2014, Bayou Corne, Louisiana, sinkhole: Precursory deformation measured by radar interferometry: Geology, v. 42, no. 2, p. 111-114.

Kuniansky, E.L., Weary, D.J., and Kaufmann, J.E., 2016, The current status of mapping karst areas and availability of public sinkhole-risk resources in karst terrains of the United States: Hydrogeology Journal, v. 24, p. 613-624.

Kim, J.W., Lu, Z., and Degrandpre, K., 2016, Ongoing Deformation of Sinkholes in Wink, Texas, Observed by Time-Series Sentinel-1A SAR Interferometry (Preliminary Results): Remote Sensing, v. 8, no. 313, doi:https://doi.org/10.3390/rs8040313.

Kim, J.W., and Lu, Z., 2018, Association between localized geohazards in West Texas and human activities, recognized by Sentinel-1A/B satellite radar imagery: Scientific Reports, v. 8, no. 4727, doi:https://doi.org/10.1038/s41598-018-23143-6.

Kim, J.W., Lu, Z., and Kaufmann, J., 2019, Evolution of sinkholes over Wink, Texas, observed by high-resolution optical and SAR imagery: Remote Sensing of Environment, v. 222, p. 119-132.

Kwoun, O., Lu, Z., Neal, C., and Wicks, C., 2006, Quiescent deformation of the Aniakchak Caldera, Alaska, mapped by InSAR: Geology, v. 34, no. 1, p. 5-8.

Linares, R., Roqué, C., Gutiérrez, F., Zarroca, M., Carbonel, D., Bach, J., and Fabregat, I., 2017, The impact of droughts and climate change on sinkhole occurrence. A case study from the evaporite karst of the Fluvia Valley, NE Spain: Science of the Total Environment, v. 579, p. 345-358.

Lu, Z., Dzurisin, D., Jung, H.S., Zhang, J.X., and Zhang, Y.H., 2010, Radar Image and Data Fusion for Natural Hazards Characterization: International Journal of Image and Data Fusion, v. 1, p. 217-242.

Lu, Z., and Dzurisin, D., 2014, InSAR imaging of Aleutian volcanoes: monitoring a volcanic arc from space, Chichester, UK: Springer Praxis Books. Geophysical Sciences. ISBN 978-3-642-00347-9: 390 p.

Lu, Z., and Zhang, L., 2014, Frontiers of Radar Remote Sensing: Photogrammetric Engineering and Remote Sensing, v. 80, no. 1, p. 5-13.

Massonnet, D., Rossi, M., Carmona, C., Adragna, F., Peltzer, G., Feigl, K., and Rabaute, T., 1993, The displacement field of the Landers earthquake mapped by radar interferometry: Nature, v. 364, p. 138-142.

Paine, J.G., Buckley, S.M., Collins, E.W., and Wilson, C.R., 2012, Assessing collapse risk in evaporite sinkhole-prone areas using microgravimetry and radar interferometry: Journal of Environmental and Engineering Geophysics, v. 17, no. 2, p. 75-87.

Qu, F.F., Lu, Z., Zhang, Q., Bawden, G.W., Kim, J.W., Zhao, C.Y., and Qu, W., 2015, Mapping ground deformation over Houston-Galveston, Texas using Multitemporal InSAR: Remote Sensing of Environment, v. 169, p. 290-306.

Rosen, P.A., Hensley, S., Joughin, I.R., Li, F.K., Madsen, S.N., Rodriguez, E., and Goldstein, R.M., 2000, Synthetic aperture radar interferometry: Proceedings of the IEEE, v. 88, no. 3, p. 333-382.

Shi, Y., Tang, Y.M., Lu, Z., Kim, J.W., and Peng, J.H., 2019, Subsidence of sinkholes in Wink, Texas from 2007 to 2011 detected by time-series InSAR analysis: Geomatics, Natural Hazards and Risk, v. 10, no. 1, p.1125-1138, DOI: https://doi.org/10.1080/19475705.2019.1566786.

Waltham, T., Bell, F., and Culshaw, M., 2005, Sinkholes and subsidence: karst and cavernous rocks in engineering and construction: Berlin, Springer, ISBN 3-540-20725-2, 383 p.

Zebker, H.A., Rosen, P.A., Goldstein, R.M., Gabriel, A., and Werner, C.L., 1994, On the derivation of coseismic displacement fields using differential radar interferometry—the Landers earthquake: Journal of Geophysical Research, 99:19617-19634.